Journal of Thermal Analysis and Calorimetry Vol. 59 (2000) 435–450

Dedicated to Prof. Edith A. Turi in recognition of her leadership in education

CRYSTALLIZATION AND MELTING OF MODEL POLYETHYLENES WITH DIFFERENT CHAIN STRUCTURES

J. A. Haigh[1], *C. Nguyen*[2], *R. G. Alamo*[2*] *and L. Mandelkern*[1]

[1]Institute of Molecular Biophysics and Department of Chemistry, Florida State University Tallahassee, FL 32306
[2]Department of Chemical Engineering, Florida Agricultural and Mechanical University and Florida State University College of Engineering, 2525 Pottsdamer St. Tallahassee, FL 32310, USA

Abstract

The crystallization and melting of three model polyethylenes of different chain structures have been studied. The polymers studied were a linear copolymer, hydrogenated poly(butadiene); a hydrogenated poly(butadiene)-atactic poly(propylene) diblock copolymer; and a three-arm star hydrogenated poly(butadiene). An important feature of this work was that the crystallizing portions of the copolymers all have the same molecular lengths.

It was found that the overall crystallization rate decreases steadily from a linear to a diblock to the star copolymer. The differences in crystallization rates are related primarily to the activation energy for segmental transport. The non-crystallizable structure affects the segmental mobility to different degrees. An estimation of this effect is presented from the analysis of the overall crystallization rates using classical nucleation theory. In spite of the differences in their molecular structure, there are no major differences in the supermolecular structure of samples crystallized rapidly or slowly cooled.

The melting process followed by DSC of the isothermally crystallized linear and star copolymers shows two endothermic peaks at intermediate undercoolings. The double melting is associated with a partitioning of crystallizable ethylene sequences during crystallization. The longest sequences are preferentially selected in the early stages of the crystallization. Single melting peaks are obtained for high and very low undercoolings for the linear and the star copolymers as well as for the diblock in the whole range of temperatures. The lack of the second, lower melting endotherm in the diblock could be associated with the influence in the crystallization process of the amorphous block in the microphase segregated melt.

Keywords: ethylene copolymers, model polyethylenes, polyethytlene crystallization, polyethylene melting, polyethylene structure-properties, random copolymers

Introduction

The polyethylenes can be synthesized to yield a variety of molecular architectures. These range from linear homopolymers and copolymers to highly ramified structures

* Author to whom all correspondence should be addressed.

1418–2874/2000/ $ 5.00
Akadémiai Kiadó, Budapest

[1, 2]. The different structures can, in turn, be expected to impart different properties to the polymers in both the molten and semi-crystalline states. Copolymerization of ethylene with alkene-type monomers has long been used to decrease the level of crystallinity of the homopolyethylene to a desired range suitable for any specific application. The properties of random ethylene-1-alkene copolymers (so-called linear low density polyethylenes) with narrow molecular mass and comonomer composition distributions have been reviewed [3]. Increasing the concentration of the comonomer decreases the melting temperature, level of crystallinity and the thickness of the resulting crystallites. A deterioration in the character of the lamellar crystallites is also observed with increasing branching content. The lamellar habit is lost in copolymers with about 4 mol% of branch points [4]. The well formed spherulites obtained in the linear homopolymers and copolymers with low branching content (1–2 mol%) become less structured with increased branching. Imperfect, randomly oriented crystals of the fringed-micelle type are the predominant morphology in the highly branched random ethylene copolymers [4, 5]. A definite correlation can be made between the lamellar and supermolecular structures [6, 7]. The properties and crystallization behavior of copolymers with butene, hexene or octene as comonomers are not significantly different from one another [8, 9]. The branches are mainly rejected into the intercrystalline regions [3, 8, 9]. Studies of the type described above have been extended in this work to random ethylene copolymers of different molecular architectures. The copolymers were synthesized by anionic polymerization [10, 11] to ensure very narrow molecular mass distribution and uniform interchain branching content.

The polymers studied here are a linear copolymer, hydrogenated poly(butadiene), an ethylene-butene random copolymer; a hydrogenated poly(butadiene)-atactic poly(propylene) diblock copolymer; and a three-arm star hydrogenated poly(butadiene). An important feature of this work is that the crystallizing portion of each of the polymers selected for study had the same molecular mass and ethyl-branching composition. We have studied the crystallization kinetics from the melt the melting behavior, the phase structure by means of DSC and density measurements, and the supermolecular structure by means of small-angle light scattering (SALS) and optical microscopy.

Experimental

Materials

The molecular characteristics of the polymers used in this work are listed in Table 1. Sample A, labeled HPBD49, is a hydrogenated polybutadiene kindly supplied to us by Graessley. Its synthesis and some properties have previously been described [10]. Sample B, designated P108, is a similar copolymer with M_w=108000 g mol^{-1}. Both of these copolymers have very narrow molecular mass and composition distributions. Samples C and D were given to us by Lohse and Fetters. Sample C, designated HPBD/APP, is a diblock copolymer of hydrogenated poly(butadiene) and atactic

poly(propylene), (hydrogenated poly(butadiene)-block-2-methyl-1,3-pentadiene). The synthesis and properties of this copolymer have been described, and was designated DEP113 [12]. Sample D, designated STAR HPBD, is a star copolymer containing 3 arms. Each arm is composed of a hydrogenated poly(butadiene) of molecular mass 50000 g mol^{-1}. It should be noted that except for P108, the molecular mass of the crystallizing entities of each of the polymers were very similar to one another, as were the short-chain branching contents.

Table 1 Molecular characteristics of the polyethylenes studied

	Type polymer	Sample designation	M_w /g mol^{-1}	M_w/M_n	Ethyl branches/100 carbons
A	Linear copolymer	HPBD49	49000	~1.1	~2.3
B	Linear copolymer	P108	108000	1.3	2.2
C	Block copolymer	HPBD/APP	54000 HPBD 59000 APP	~1.2	2.0
D	Star copolymer	STAR/HPBD	150000 (50000 each arm)	~1.2	2.0

Sample preparations

Samples for study were initially pressed into thin films between Teflon sheets at ca 150°C in a Carver press. For one mode of crystallization the films were held at 150°C for approximately 2 min before being quenched quickly in a dry ice/2-propanol mixture at –78°C. These samples were used for SALS, density, microscopy and DSC studies. In the other mode of crystallization, the samples were crystallized isothermally at elevated temperatures for extended time periods. For this procedure, films were placed in glass tubes which were evacuated and sealed. The sealed tubes were immersed for 15 min in an oil bath set at a temperature of 150°C to ensure complete melting and then transferred to a second pre-set oil bath and held there for the desired time. Samples were crystallized in this way at 90°C for 7 days and at 95.4°C for 16 days. After the period of crystallization the tubes were quickly transferred to a dry ice/2-propanol bath at –78°C.

Procedures

The enthalpy of fusion, ΔH_f and the melting temperature, T_m, were determined with a Perkin Elmer DSC-2B differential scanning calorimeter operating at a heating rate of 10°C min^{-1}. The instrument was calibrated using indium as a standard. Since the melting behavior of the samples investigated occurs over a broad temperature range, the instrument was fitted with a low temperature accessory. ΔH_f was calculated from the area of the melting endotherms and was converted to the degree of crystallinity, $(1–\lambda)_{\Delta H}$, by taking the enthalpy of fusion of a perfect polyethylene crystal to be 69 cal g^{-1} [13].

The same instrument was utilized for the crystallization kinetics measurements. Samples weighing approximately 3 mg were placed in aluminum pans and heated to 148.2°C for 5 min. They were then cooled rapidly in the DSC (nominally at 320 K min^{-1}) to a fixed crystallization temperature. For the lowest crystallization temperatures, the crystallization exotherm was recorded. However, as the crystallization temperature was raised, and the rate of crystallization reduced, the exotherm measurement became inaccurate, as well as impractical, so an alternative method was adopted. The samples were crystallized for increasing lengths of time and then melted at a rate of 10°C min^{-1}. As has been found in other studies, there was good agreement between the isotherms obtained by the exotherm and endotherm methods [14]. The time taken to reach 10% of the maximum crystallinity level, ($\tau_{0.1}$), was determined for each isotherm and taken as a measure of the crystallization rate.

The melting of crystals formed isothermally was also followed as a function of crystallization time. In this experiment consecutive crystallizations at the same temperature (T_c) were repeated for increasing times and the melting obtained at 10°C min^{-1} from the T_c.

Densities were measured in a trimethylene glycol/2-propanol density gradient column at 23°C [15]. The column was calibrated with glass float standards. The densities were converted to degrees of crystallinity, $(1–\lambda)_d$, using the known specific volume relationship [16]. The density of crystalline polyethylene was taken as 1.00 g cm^{-3}, and that of amorphous polyethylene as 0.853 g cm^{-3}.

The small-angle light scattering patterns, that served as the main basis for characterizing the supermolecular structures, were obtained with an instrument that has been described previously [17]. The H_v pattern was used for this purpose. The radius of the spherulites was calculated from the Eq. [17]

$$U_{max} = \frac{4\pi R}{\lambda}\left(\sin\frac{\theta_{max}}{2}\right) \quad (1)$$

where U_{max} is the maximum scattering in the radial direction and equals 4.1, R is the spherulitic radius, λ is the wavelength of radiation, and θ_{max} is the angle at which maximum scattering occurs. The optical micrographs were obtained with Leitz microscope fitted with an automatic photographic camera.

Results and discussion

Crystallization kinetics

The crystallization kinetics studies were undertaken to assess the role of the molecular architecture on the rates. The isotherm shapes of the copolymers were similar to one another and to those previously published for the linear copolymer [18]. The natural log, ln, of the crystallization rate, defined as the inverse of the time required to obtained 10% of the maximum crystallinity ($1/\tau_{0.1}$), is plotted in Fig. 1 *vs*. the crystallization temperature for each of the polyethylenes studied. The rates measured from

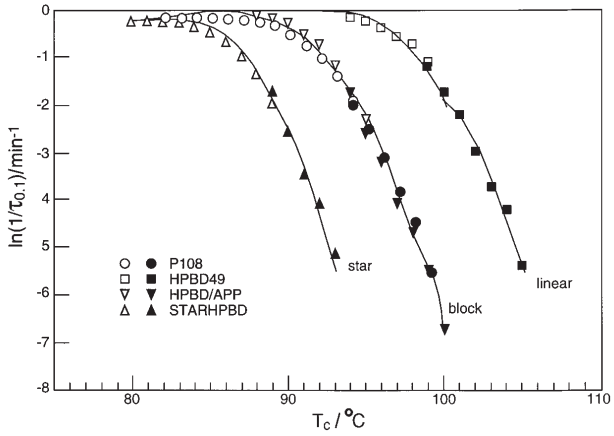

Fig. 1 Plot of ln of crystallization rate ($1/\tau_{0.1}$) *vs*. the crystallization temperature for indicated polyethylenes

exotherms, and represented by the open symbols, merge smoothly with the endothermic ones, that are represented by the solid symbols. It is clear from this figure that the molecular architecture has a pronounced influence on the rate. Although the shapes of the plots are qualitatively similar to one another, the time scales are quite different. The two linear copolymers, samples A and B, follow the pattern previously reported [18]. The lower molecular mass linear copolymer, sample A, crystallized at a much faster rate than the higher molecular mass (sample B) at the same temperature. Sample A also crystallized much faster than sample C, the block copolymer, although the crystallizing block had a very similar molecular mass. The three-arm star copolymer, whose arms are each also of similar molecular mass, crystallized at an even slower rate. The chain structure has an obvious and major influence on the crystallization rate. The melts of samples A, B, and D are homogeneous. However, the symmetric diblock copolymer, sample C, has been reported to undergo microphase separation in the melt, the phases being strongly segregated [12]. The crystallization rates of sample B and the di-block copolymer are, coincidentally, very close to one another.

As is typical of polymer crystallization, the crystallization rates of all the polymers given in Fig. 1 exhibit a strong negative temperature coefficient, indicative of a nucleation controlled process in this temperature range. Using the Turnbull-Fischer [19] expression for the steady state nucleation rate we can express the overall crystallization rate as

$$1/\tau_{0.1}=k_0 \exp\left\{\left(\frac{-E_D}{RT}\right)\left(\frac{\Delta G^*}{RT}\right)\right\} \quad (2)$$

where k_0 is a constant, ΔG^* is the free energy of forming a nucleus of critical size and E_D represents the effective activation energy of segmental transport across the liquid-crystal interface. Equation (2) is very general so several assumptions have to be made in order to use it to analyze the experimental data.

The strong temperature coefficient arises from the temperature dependence of ΔG^*. The detailed form of ΔG^* is dependent on the specific type of nucleus that is formed, and on the nucleation process. Several types of nucleation processes can be considered [20, 21]. These include the formation, either homogeneous or heterogeneous, of three-dimensional nuclei, or a Gibbs-type two-dimensional coherent unimolecular nucleus. It has been shown for the crystallization of many polymers that it is not possible to discriminate between the formation of either a two- or three-dimensional nucleus. Therefore, in order to analyze the data according to nucleation theory an assumption has to be made. We take as an example a two-dimensional coherent nucleation process. The major conclusions reached do not depend in any way on either the type of nucleus that is selected for analysis or on the chain structure within the nucleus [22]. We choose this nucleation model solely for illustrative purposes.

The expression for ΔG^* of a random copolymer, where only one of the comonomers participates in the crystal has been given. Adapted to a unimolecular, coherent nucleus, it can be expressed as [18]

$$\Delta G^* = \frac{4\sigma_{en}\sigma_{un}}{\Delta G_u + RT\ln X_A} \tag{3}$$

with ΔG_u the free energy of fusion per repeating unit. This quantity can be approximated by $\Delta H_u(T_m^o - T)/T_m^o$ in the vicinity of T_m^o. Here ΔH_u is the heat of fusion per repeating unit, T_m^o is the equilibrium melting temperature of the infinite molecular mass homopolymer, σ_{en} is the interfacial free energy for nucleation of the surface normal to the chain axis, σ_{un} is the corresponding lateral surface free energy per repeating unit and X_A is the mole fraction of crystallizable units.

Since there is no fundamental theoretical expression for the transport term several arbitrary forms have been considered. It has been successfully expressed in terms of the simple Arrhenius form over a limited range of crystallization temperatures [23]. In this case Eq. (2) will apply. More generally, over an extended temperature range, the Vogel equation has been used to express the transport term. In this case, Eq. (2) is written as

$$\ln(1/\tau_{0.1}) = \ln K_0 - \frac{U^*}{R(T - T_\infty)} - \frac{4\sigma_{en}\sigma_{un}}{RT(\Delta G_u + RT\ln X_A)} \tag{4}$$

Here U^* plays the role of an activation energy. T_∞ is the temperature below which segmental motion becomes infinitely slow. It is conveniently defined as $T_\infty = T_g - C_2$, where T_g is the glass temperature and C_2 is an arbitrary constant. Equation (4) can then be written as

$$\ln(1/\tau_{0.1}) = \ln K_0 - \frac{U^*}{R(T - T_g + C_2)} - \frac{4\sigma_{en}\sigma_{un}}{RT(\Delta G_u + RT\ln X_A)} \tag{5}$$

In this equation, it is tacitly assumed that crystallization is taking place in Regime I. For crystallization in Regime II, the factor 4 in the last term in Eq. (5) is replaced by 2.

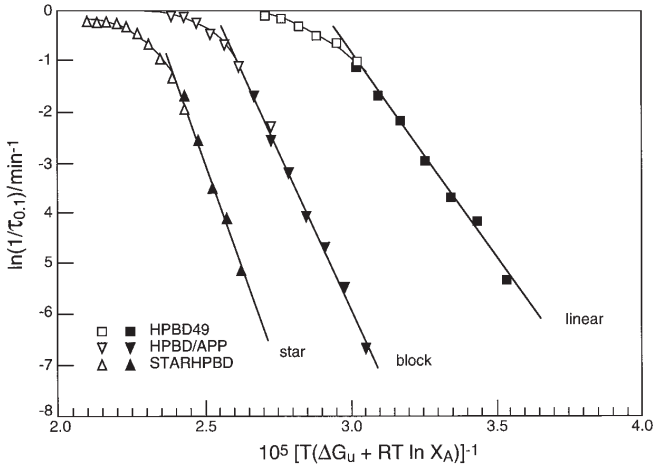

Fig. 2 Plot of ln of crystallization rate ($1/\tau_{0.1}$) *vs*. the temperature function according to Eq. (5)

We can now analyze the kinetic data in terms of Eq. (5). However, it is important to keep in mind the basic assumptions made with regard to both ΔG^* and to the transport term. As a first step in the analysis, the experimental data from Fig. 1 are plotted in Fig. 2 according to Eq. (5) with neglect of the transport term. In constructing this figure ΔH_u was taken to be equal to 950 cal mol^{-1} and T_m^o was taken as 145.5°C [24]. Not surprisingly, the difference in crystallization rates between the three structures is still maintained in this figure. The data in the high temperature region can be represented by a linear relation. At the lower crystallization temperature, deviations occur as the crystallization rates become very rapid. In analyzing the data it is assumed that the crystallization is taking place in Regime II. Hence, the slope of the straight line that represents the high temperature data is equal to $-(2\sigma_{un}\sigma_{en})/R$. From this data the product of the interfacial free energies σ_{en} σ_{un} can be obtained. This product is given in Table 2 for the copolymers with the same crystallizable length. The corresponding values of σ_{en} are also listed with the assumption that σ_{un} is 100 cal mol^{-1} for each of the polymers. The product of interfacial energies, or of σ_{en}, increases approximately two-fold from the linear copolymer to that of the star. The value of σ_{un} σ_{en} obtained here for HPBD49 is in very good accord with the value of $7.41 \cdot 10^5$ cal^2 mol^{-2}, that has been previously reported for the same copolymers based on dilatometric kinetic studies [18].

Table 2 Interfacial free energies deduced from Fig. 2

Sample	10^{-5} $\sigma_{un}\sigma_{en}$/cal^2 mol^{-2}	$\sigma_{en}(\sigma_{un}=100)$/cal mol^{-1}
HPBD49	8.0	8000
HPBD/APP	12.0	12000
STAR/HPBD	17.2	17200

The increase in σ_{en} that is deduced for the star and block copolymers relative to the linear copolymer can be attributed to the disorder at the crystal-amorphous interface. Although the three polymers have very similar branching, or counit contents, the star and the block copolymers have additional structural features that can not be incorporated into the nucleus. For the block copolymer it is the junction with the amorphous block, while for the star it is the region surrounding the junction point where the three chains meet.

Analysis of the data using either of the transport terms, with either a fixed E_D or U^*, for each of the polymers leads to essentially the same results described and illustrated in Fig. 2. Put another way, because of the limited range in isothermal crystallization temperatures that can be studied with the polyethylenes, and the domination of the nucleation term in Eq. (5), the role of the transport term in each of the systems is minimal. However, the fact that the polymers show significantly different rates at the same undercooling is indicative of very different energy barriers for segmental transport. The difference in the magnitudes of this energy between samples A, C and D can be estimated by choosing values of E_D or U^* that lead to continuous curves. These curves are shown in Figs 3 and 4 for the Arrhenius and Vogel type transport terms respectively. The arbitrary constants that are needed are given in Table 3. Only one parameter is needed to construct Fig. 3 while two parameters are required for Fig. 4. In this case the constant C_2 was arbitrarily kept constant at 30 K. Except for the low temperatures, that involve very rapid crystallizations, the crystallization rates can be juxtaposed for the different structures studied. To accomplish this the activation energy has to be increased in going from the linear copolymer to the three arm-star. This re-

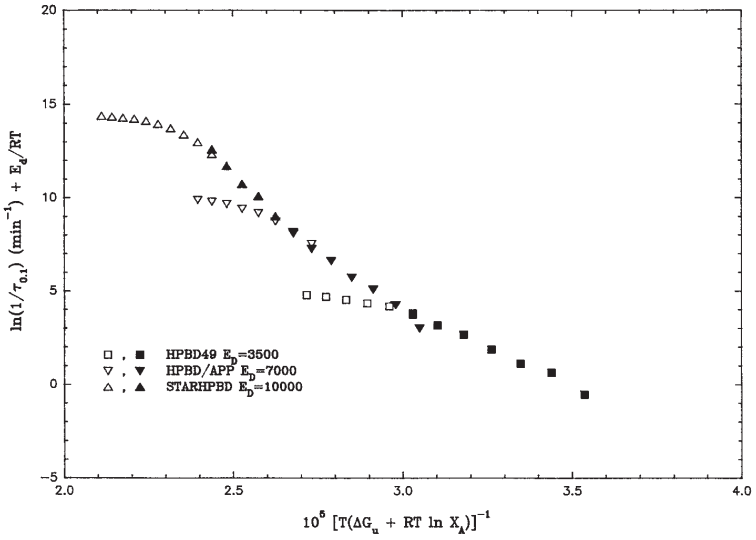

Fig. 3 Plot of ln of crystallization rate ($1/\tau_{0.1}$) plus Arrhenius type transport term *vs.* temperature function $\times 10^5$. Values of E_D used to obtain juxtaposition of curves are indicated

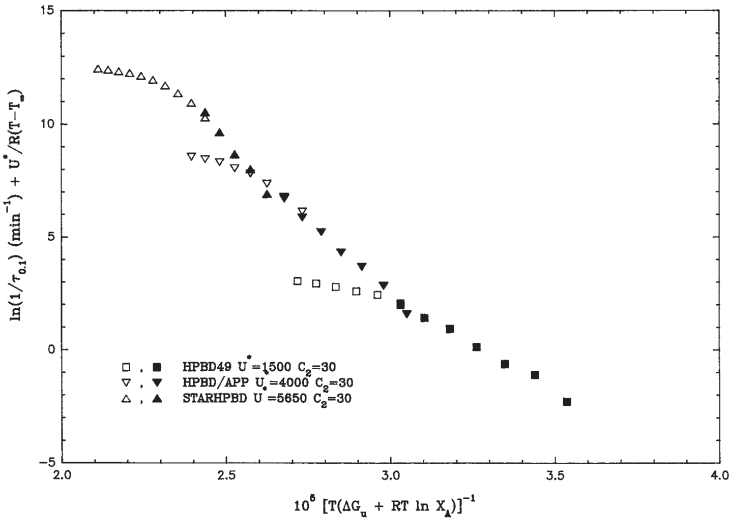

Fig. 4 Plots of ln of crystallization rate ($1/\tau_{0.1}$) plus Vogel type transport term *vs*. temperature function $\times 10^5$. Values of U^* and C_2 used to obtain juxtaposition of curves are indicated

sult is physically satisfactory since the long-chain branches in the star polymer would be expected to retard the transport, or diffusion of the crystallizing units to the interface. The transport of the segment of the block copolymer would be expected to be between those of the linear polymer and the star. To obtain a continuous curve the block copolymer required values of E_D or U^* that are approximately double the values taken for the linear copolymer (HPBD49). The star required values about three times those of the linear. The differences in slopes are still discerned in this juxtaposition.

Table 3 Parameters used to construct Figs 3 and 4

Sample	Arrhenius factor (E_D)/ cal mol^{-1}	U^*/cal mol^{-1}	C_2/K
HPBD49	3500	1500	30
HPBD/APP	7000	4000	30
STAR/HPBD	10000	5650	30

The temperature coefficients of the crystallization kinetics of the three polyethylene structures that have been studied are quite different from one another. The differences in time scale can be related primarily to the activation energy for segmental transport. There are also differences in the interfacial free energy required to form a nucleus of critical size. The parameters involved for each of the polymers can be related, in a qualitative manner, to their molecular architectures. Taking the linear copolymers as a reference, the segmental mobility of the diblock copolymer is retarded by the heterogeneous nature of its melt. Long-chain branches, known to retard seg-

mental mobility, are manifest in the three-arm star, which is the slowest to crystallize. The character of the interphase, and the value of σ_{en}, are also influenced by the non-crystallizable structures.

Phase structure

The phase structure of the model polyethylenes is described here by the degree of crystallinity determined from both the density and enthalpy of fusion, their comparison, and a determination of the supermolecular structure. Two different modes of crystallization were involved. In one, the samples were isothermally crystallized at a predetermined temperature and then rapidly quenched to –78°C. In the other, the samples were directly quenched from the melt. The levels of crystallinity thus determined are given in Table 4.

Table 4 Crystallinity levels as determined from enthalpy of fusion and density

Sample	Crystallinity from DSC/$(1-\lambda)_{\Delta H}$[(a)]	Crystallinity from density/$(1-\lambda)_d$	Melting temperature/°C[(b)]
HPBD49 (90°C)	34		107
HPBD49 (95.4°C)	29		103.6, 107.6
HPBD49 (quench)	24	43	103
STAR/HPBD (90°C)	25	37	97
STAR/HPBD (95.4°C)	24		102.6
STAR/HPBD (quench)	22	35	95
HPBD/APP (90°C)	35		105
HPBD/APP (95.4°C)	32		107.3
HPBD/APP (quench)	19		103

[(a)] The value of $(1-\lambda)_{\Delta H}$ includes the contribution from all endotherm peaks
[(b)] The melting temperature corresponding to the quenched peak has been omitted for clarity

The results are similar to those previously reported for linear ethylene-1-alkene copolymers [8, 9, 25]. The levels of crystallinity depend on the mode of crystallization. The values obtained after isothermal crystallization are greater than for the quenched samples. Of most interest is the fact that the values of $(1-\lambda)_d$ are greater than $(1-\lambda)_{\Delta H}$. This result has been observed previously for ethylene copolymers [9, 26], linear polyethylene [27] as well as other polymers [28, 29]. The differences, that range from 0.12 to 0.19, for the copolymers studied here can be attributed to contributions from the interfacial region [28]. Independent methods of assessing the interfacial regions for the polyethylenes agree with these values.

A description of the supermolecular structure, as observed by SALS and optical microscopy, is given in Table 5. Both methods give essentially the same results. The change in supermolecular structure with crystallization temperature follows the pattern previously established [6, 30]. No describable structures are observed for rapidly crystallized, quenched samples. Better organized spherulitic structures are observed

as the isothermal crystallization temperature is increased. Quite surprisingly, there are not major differences between the different molecular architectures when compared under the same crystallization conditions.

Table 5 Supermolecular structures

Sample	Microscope observations	Small angle light scattering
HPBD49 (90°C)	spherulites	no pattern
HPBD49 (95.4°C)	spherulites	no pattern
HPBD49 (quenched)	no structure	no pattern
STAR/HPBD (90°C)	spherulites	spherulites: radius 3.7 μm
STAR/HPBD (95.4°C)	spherulites	no pattern
STAR/HPBD (quench)	no structure	no pattern
HPBD/APP (90°C)	faint areas of disordered spherulites	no pattern
HPBD/APP (95.4°C)	spherulites	no pattern
HPBD/APP (quench)	no structures	no pattern

Melting behavior

The cooling curves from the melt of the linear and diblock copolymers have been previously reported [12]. The main exothermic peaks, representing crystallization, are very similar for these two polymers. On the other hand, the star copolymer crystallizes at a lower temperature. All three polymers also display a small exothermic peak at lower temperatures. This temperature is around 65°C for the linear and diblock copolymers and 55°C for the star copolymer. This secondary exotherm is observed in most linear low density polyethylenes but not in the linear homopolymer. It has been interpreted to be a consequence of the crystallization of a small number of short sequences confined to the interlamellar regions. The melting curves of the model copolymers after cooling from the melt at 10° min^{-1} are shown in Fig. 5. Interestingly, only a single endothermic melting peak is observed in Fig 5. indicating the presence of a broad distribution of crystal thicknesses in the slowly cooled samples.

The melting temperatures of the quenched samples are also listed in Table 4. The values for the linear and block copolymers are identical suggesting that, in fact, the diblock copolymer presents microphase separation in the melt and that the phases are strongly segregated. It is envisaged that relatively rapid crystallization freezes the lamellar structure present in the melt with little interference of the amorphous block. The crystallite structure developed is, thus, no different from that of the linear copolymer. The melting temperature of the star copolymer is approximately 8°C lower. If the crystallite thicknesses are the same for the three polymers this decrease in T_m can be attributed to an increase in the interfacial free energy, σ_{en}, of the mature crystallite. The junction of the three arms, that is confined to the amorphous region, affects significantly the topology and random defect composition distribution in this phase and,

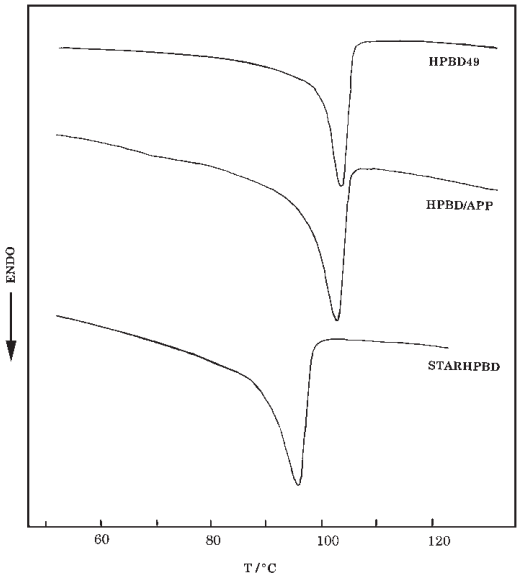

Fig. 5 Melting curves for model copolymers crystallized by cooling from the melt at 10 K min^{-1}. Heating rate 10 K min^{-1}

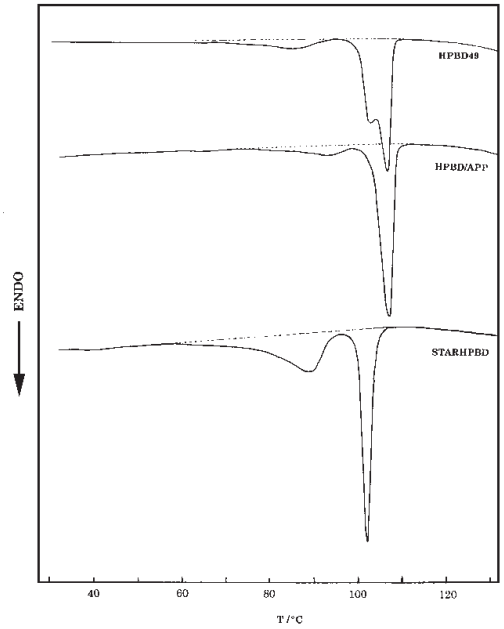

Fig. 6 Melting curves for model copolymers isothermally crystallized at 95.4°C and subsequently quenched. Heating rate 10 K min^{-1}

thus, the formation and melting of the crystallites. Melting of samples quenched to –78°C resulted in very similar endotherms as those Fig. 5.

The isothermally crystallized samples present some interesting features. In a series of experiments the three copolymers were crystallized at 95.4°C in sealed glass tubes and subsequently quenched in dry ice/2-propanol. The resulting melting curves are shown in Fig 6. The low temperature endotherms at 85, 93 and 98°C respectively, correspond to melting of the crystals formed on cooling. They are not of particular interest in the present context. The crystals formed isothermally from the diblock and star copolymers melt sharply as single peaks. The melting temperature of the star is 5°C lower than that of the diblock. The linear copolymer presents bimodal melting behavior and the value of the highest melting temperature is identical to the melting temperature of the block. The degree of crystallinity developed isothermally by the linear copolymer or the block is also basically identical, 23 and 24% respectively. The slower crystallization kinetics of the star copolymer hindered the development of crystallinity at 95.4°C for the same crystallization time. However, when the content of crystals formed on cooling is added to that formed isothermally, the degrees of crystallinity of the three polymers are very similar as indicated in Table 4. Isothermal crystallization at 90°C, followed by quenching, gave very similar curves. The melting temperatures were slightly lower than for the higher temperature crystallization but the differences were comparable.

The evolution of the melting endotherms with crystallization time shows some unusual and unique features. Examples of this development are shown in Fig. 7 for each of the model copolymers studied. In these experiments the fusion process was started from the crystallization temperatures, without any cooling. The fusion of the linear and star copolymers are separated by about 5°C. Initially only the high melting peak is observed, the intensity of which increases with time. The low melting peak develops subsequently and its intensity increases very rapidly. Only single peaked endotherms, whose intensities increase with time, are observed for crystallization temperatures above 103°C for the linear copolymer and above 93°C for the three-arm star copolymer. In a similar manner only a single endothermic peak is observed after rapid crystallization at low temperature. There is thus a window, or interval of crystallization temperatures, that allows for the development of the two melting peaks in these two copolymers. Two melting peaks have been reported previously for isothermally crystallized linear copolymers [31].

The temperature restriction on the development of the two peaks suggests that the undercooling plays an important role, and governs the sequences that can participate in the crystallization. At the high crystallization temperatures only the longest sequences can participate. The undercooling will be too low to allow the shorter sequences to participate in the nucleation process. At the low crystallization temperatures the nucleation restraint will be minimal so that effectively most of the sequences can participate, resulting in only one endothermic peak. At the intermediate crystallization temperatures, the longest sequences, being at a larger undercooling will crystallize first. The shorter sequences, being at an effectively small undercooling, will crystallize at a slower but steady

rate. Besides nucleation barriers the crystallization of the shorter sequences may also be affected by segmental mobility, that will be decreased by the crystallization of the longest sequences. As a consequence, within this window of crystallization temperatures two endothermic peaks will result, each representing different populations of crystallizable sequences and thus crystallite sizes. Similar results with other random ethylene copolymers, and a more detailed analysis, will be presented shortly.

Recently, two melting peaks were reported in hydrogenated poly(butadienes) that were isothermally crystallized for ten min [32]. These results were explained by a model that allows the crystallizable sequences to be partioned into two fractions based on lengths established by crystallization temperature and kinetics. The Gibbs- Thomson equation was used to establish the crystallite thicknesses at the crystallization and melting temperatures. These were then related to the respective sequence length.

In contrast to the results for the linear and star copolymers shown in Fig. 7, the melting curves for the diblock polymer only give a relatively sharp, single endothermic peak. Experiments at other temperatures, over the isothermal crystallization range, give similar results. It is tempting to attribute the lack of the second, lower melting endotherm to the influence of the amorphous block in the microphase segregated melt. Preliminary crystallization and melting studies with a similar diblock, but one that has a homogeneous melt [33, 34] has yielded two melting endotherms similar to those shown by the linear and star copolymers. One would expect that with the restricted crystallization, the level of crystallinity of the diblock shown in Fig. 7 would be lower than the linear copolymer. However, as is shown in Table 4, both poly-

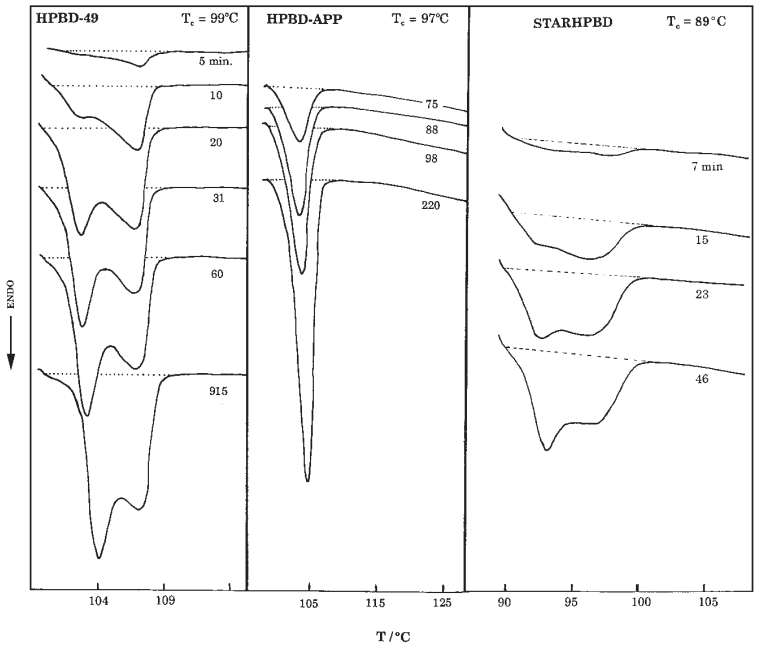

Fig 7 Melting curves for isothermal crystallization at the indicated temperatures after different crystallization times. Heating rate 10 K min^{-1}

mers develop comparable levels of crystallinity. A more extensive study, with a variety of block copolymers with different melt structures, are needed in order to understand the results with the diblock copolymer that was studied here.

Attempts to establish the equilibrium melting temperatures of the copolymers studied here by means of T_m/T_c extrapolation failed. The results obtained were very similar to those reported previously for a set of random ethylene copolymers [35]. These results, and those reported previously, emphasize the impossibility of using the Hoffman-Weeks extrapolation method [36] to obtain the equilibrium melting temperature of these types of random copolymers. The composition of the melt in these types of copolymers changes during melting.

Conclusions

Model random ethylene copolymers of different molecular architectures and identical crystallizing portions of the chain show differences in their crystallization behavior. The overall crystallization rate decreases steadily from a linear to a diblock and to a star copolymer. The differences in crystallization rates are related primarily to the activation energy for segmental transport. Taking the linear copolymer as a reference, the segmental mobility of the diblock copolymer is retarded by the heterogeneous nature of its melt. A retardation in the rate of the three arms star is given by the long-chain branch nature of this copolymer. The non-crystallizable structure also affects the crystalline amorphous interphase and value of the basal interfacial free energy of the nucleus that develops.

In spite of the differences in their molecular structure, there are not major differences in the supermolecular structure of samples crystallized rapidly or slowly cooled.

The melting process followed by DSC of the isothermally crystallized linear and star copolymers shows two endothermic peaks at intermediate undercoolings. The double melting is associated with a partitioning of crystallizable ethylene sequences during crystallization. The longest sequences are preferentially selected in the early stages of the crystallization. Single melting peaks are obtained for high and very low undercoolings for the linear and the star copolymers as well as for the diblock in the whole range of temperatures. The lack of the second, lower melting endotherm in the diblock could be associated with the influence in the crystallization process of the amorphous block in the microphase segregated melt.

* * *

This work was funded by the National Science Foundation Polymer Program (DMR-94-19508) whose aid is gratefully acknowledged. The REU program of the National Science Foundation allowed C. Nguyen, a Chemical Engineering undergraduate student to participate in this research.

References

1 S. A. Miller, Ed., Ethylene and Its Industrial Derivatives. Ernest Been Limited, London 1969.
2 L. Mandelkern, R. G. Alamo, G. D. Wignall and F. C. Stehling, Trends in Polymer Science, 4 (1996) 377.

3 R. G. Alamo and L. Mandelkern, Thermochim. Acta, 238 (1994) 155.
4 I. G. Voigt-Martin, R. Alamo and L. Mandelkern, J. Polym. Sci., Polym. Phys. Ed., 24 (1986) 1283.
5 S. Bensason, J. Minick, A. Moet and E. Baer, J. Polym. Sci., Polym. Phys., 34 (1996) 1301.
6 L. Mandelkern, M. Glotin and R. S. Benson, Macromolecules, 14 (1981) 22.
7 F. Chowdhury, J. A. Haigh, L. Mandelkern and R. G. Alamo, Polymer Bulletin, 41 (1998) 463.
8 R. G. Alamo and L. Mandelkern, Macromolecules, 22 (1989) 1273.
9 R. G. Alamo, B. D. Viers and L. Mandelkern, Macromolecules, 26 (1993) 5740.
10 H. Rachapudy, G. G. Smith, V. R. Raju and W. W. Graessley, J. Polym. Sci., Polym. Phys. Ed., 17 (1979) 1211.
11 Z. Xu, J. W. Mays ansd X. Chen, N. Hadjichristidis, N. F. Schelling, H. E. Blair, D. S. Pearson and L. Fetters, Macromolecules, 18 (1985) 2560.
12 K. Sakurai, W. J. MacKnight, D. J. Lohse, D. N. Schulz and J. A. Sissano, Macromolecules, 27 (1994) 4941.
13 F. A. Quinn, Jr. and L. Mandelkern, J. Amer. Chem. Soc., 80 (1958) 3178.
14 M. J. Galante, L. Mandelkern, R. G. Alamo, A. Lehtinen and R. Paukkeri, J. Thermal Anal., 47 (1996) 913.
15 J. G. Fatou and L. Mandelkern, J. Phys. Chem., 69 (1965) 417.
16 R. Chiang and P. J. Flory, J. Amer. Chem. Soc., 83 (1961) 2857.
17 J. Maxfield and L. Mandelkern, Macromolecules, 10 (1977) 1141.
18 R. G. Alamo and L. Mandelkern, Macromolecules, 24 (1991) 6480.
19 D. Turnbull and J. C. Fischer, J. Chem. Phys., 17 (1949) 71.
20 L. Mandelkern, J. G. Fatou and C. Howard, J. Phys. Chem., 68 (1964) 3386.
21 L. Mandelkern, J. G. Fatou and C. Howard, J. Phys. Chem., 69 (1965) 956.
22 L. Mandelkern, N. L. Jain and H. Kim, J. Polym. Sci. A-2,6 (1968) 165.
23 N. Okui, in Crystallization of Polymers, NATO ASI Series C: Mathematical and Physical Sciences, M. Dosière, Ed., Kluwer Acad. Pub., 1995, p. 593.
24 P. J. Flory and A. Vrij, J. Amer. Chem. Soc., 85 (1963) 3548.
25 R. Alamo, R. Domszy and L. Mandelkern, J. Phys. Chem., 88 (1984) 6587.
26 S.-D. Clas, R. D. Heyding, D. C. McFaddin, K. E. Russell, M. V. Scammell-Bullock, E. C. Kelusky and D. St-Cyr, J. Polym. Sci., Polym. Phys. Ed., 26 (1988) 1271.
27 M. Glotin and L. Mandelkern, Colloid. Polym. Sci., 260 (1982) 182.
28 L. Mandelkern, Chemtracts-Macromolecular Chemistry, 3 (1992) 347.
29 J. R. Isasi, L. Mandelkern, M. J. Galante and R. G. Alamo, J. Polym. Sci., Ed. Part B: Polym. Phys., 37 (1999) 323.
30 M. Glotin and L. Mandelkern, Macromolecules, 14 (1981) 1394.
31 R.G. Alamo, L. Lu and L. Mandelkern, Polym. Preprints, 35 (1994) 410.
32 B. Crist and D. N. Williams, J. Macromol Sci. Phys., 1999, in press.
33 The single phase melt diblock studied was sample 30/78 listed in Table 1 of reference [34]. It is a hydrogenated poly(butadiene) hydrogenated 1,4-isoprene diblock copolymer.
34 P. Rangarajan, R. A. Register and L. J. Fetters, Macromolecules, 26 (1993) 4640.
35 R. G. Alamo, E. K. M. Chan, L. Mandelkern and I. G. Voigt-Martin, Macromolecules, 25 (1992) 6381.
36 J. D. Hoffman and J. J. Weeks, J. Res. Natl. Bur. Stand. Part A, 66 (1962) 13.